Band structures and native defects of ammonia borane

D. West,[1,*] Sukit Limpijumnong,[2] and S. B. Zhang[1]
[1]*Physics Department, Rensselaer Polytechnic Institute, Troy, New York 12180, USA*
[2]*School of Physics, Suranaree University of Technology and Synchrotron Light Research Institute, Nakhon Ratchasima 30000, Thailand*
(Received 17 December 2008; published 24 August 2009)

Band structures and native defects in molecular solid ammonia borane (AB) are investigated by using first-principles calculations based on the density-functional theory (DFT). The native defects include NH_3 and BH_3 antisites, interstitials, and vacancies in the various charge states. Despite that the AB crystal is an insulator with a DFT band gap larger than 6 eV, some of the charge-neutral native defects can be abundant, especially at the NH_3-rich growth conditions, due to their exceptionally low formation energies. This is in sharp contrast to defects in semiconductors for which the formation energies of charge-neutral defects are usually high and correspondingly the concentrations of those defects are low.

DOI: 10.1103/PhysRevB.80.064109 PACS number(s): 61.72.−y, 71.15.Mb, 71.20.−b

I. INTRODUCTION

Ammonia borane (AB), also known as borazane, is a molecular solid at room temperature with a unit cell of NH_3BH_3 molecules. It has recently received considerable attention due to its high hydrogen content (19.6 wt %), which offers a good deal of promise as a candidate for onboard hydrogen storage applications.[1] Furthermore, its volumetric energy density (4.94 kWh/L) is superior to that of liquid hydrogen (2.36 kWh/L). The AB solid is stable at room temperature, with a melting point of 383–388 K.[2,3] The formation of solid is originated from the difference in the electronegativity between B and N. The electronegative N takes electrons from its three neighboring H atoms, leaving a partial positive charge. The electropositive boron, on the other hand, gives electrons away to its three neighboring H atoms, leaving a partial negative charge. The solid is held together due to the attraction between the opposite charges on the hydrogen atoms, or dihydrogen bonds. On average, each AB molecule has six dihydrogen bonds. At sufficiently low temperatures, the AB solid forms ordered orthorhombic phase. In this phase, the NH_3BH_3 molecules are locked into position and are unable to rotate. At 225 K, however, the ammonia borane undergoes an order-disorder phase transition[4,5] to form a new tetragonal phase.

There have been several thermal decomposition studies of the ammonia borane.[6–9] These studies consistently showed that the thermal decomposition of NH_3BH_3 takes place in two exothermic steps, each of which releases a formula unit of H_2. The first step is the creation of the H_2 and polyaminoborane (PAB), i.e., $(NH_3BH_3)_x \rightarrow (BH_2NH_2)_x + xH_2$. This reaction has an associated $\Delta H = -0.22$ eV per H_2. Although the reaction is exothermic, a barrier exists so thermal energy is required for the reaction to move forward. It is found that the second step of the decomposition starts at temperatures near 150 °C. The second step is the continued decomposition of PAB to H_2 and polyiminoborane (PIB), following the reaction: $(NH_2BH_2)_x \rightarrow (NHBH)_x + xH_2$. Further decomposition requires a much higher temperature than that suitable for hydrogen storage. While the first step in this decomposition occurs very rapidly[7] at the boiling point of AB (114 °C), it is relatively slow in the temperature regime suitable for onboard H storage, which is 30–85 °C.[10]

Increasing reaction kinetics at low temperature is a very active area of research. Ball milling and doping the AB materials have shown some promise.[11] AB in solutions has been studied in the form of acid-catalyzed[12] and transition-metal-catalyzed[13] AB or solvated AB in ionic liquids.[14] With transition-metal catalysis, it is possible to get up to nearly 2.5 H_2 off NH_3BH_3.[13] The AB material can also be embedded in porous matrices, both in nanoscaffolds of mesoporous silica[9] and in carbon cryogels,[15,16] which has been shown to markedly improve the kinetics and thermodynamics of the H desorption. Moreover, the replacement of hydrogen by lithium and sodium in the form of NH_2LiBH_3 and NH_2NaBH_3 has been suggested[17] to accelerate the reaction kinetics.

First-principles studies ranging from density-functional theory (DFT) (Refs. 18 and 19) to quantum chemistry[20–23] calculations have been performed in the past to determine the reaction paths and energetics of H desorption. While this is a very important problem, none of the previous works considered the potential role of defects. As a matter of fact, for all hydride materials there are only a few studies of defects in hydrogen release systems. For hydride materials that are insulators with considerable band gaps, native defects might not play an important role. It is known that for wide-band-gap materials, neutral native defects are high in energy and only charged defects can have reasonably low formation energies at certain Fermi levels. Under *p*-type conditions where the Fermi level is near the valence-band edge, some positively charge native defects (donors) may have low energy. On the other hand, under *n*-type conditions, where the Fermi level is near the conduction-band edge, some negatively charged native defects (acceptors) may have low energy. In an insulator, however, the Fermi level is located in the gap, far away from both valence-band and conduction-band edges; resulting in no native defects with low energy. Therefore, it may be reasonable to ignore the effects of native defects on those materials.

The purpose of this work is to contribute to the fundamental understanding of the material properties of AB solid. We consider the AB solid here because as a molecular solid, its physical behavior can be qualitatively different from many other hydrides. Indeed, our calculation shows that unlike a typical wide-gap semiconductor, the formation energy of a

charge-neutral native defect in the AB solid can be exceptionally low. For example, under the BH_3-rich growth condition, charge-neutral BH_3 interstitial has a formation energy of only 0.75 eV. Under the NH_3-rich growth condition, charge-neutral NH_3 interstitial and antisite have the formation energy of 0.3 and 0.2 eV, respectively. The formation energy of BH_3 vacancy is even 0.1 eV negative. The physical reason for the exceptionally low defect formation energies can be traced back to the relatively low cohesive energy of molecular solids.

II. COMPUTATIONAL METHOD

Our calculations have been carried out using density-functional theory within the generalized gradient approximation (GGA) of Wang and Perdew (PW91) (Ref. 24) and projector augmented wave (PAW) pseudopotentials,[25,26] as implemented in the Vienna *ab initio* simulation package (VASP) codes.[26–29] In the calculations, the solutions to the generalized self-consistent Kohn-Sham equations are calculated using an efficient matrix-diagonalization routine based on sequential band-by-band residual minimization method and Pulay-like charge-density mixing.[30] We used a plane-wave basis set with the cutoff energy of 400 eV in all calculations. For defects, a supercell approach was used with the supercell size of 128 atoms, i.e., 16 NH_3BH_3 molecules. To find the optimized configuration of each defect, all atoms are allowed to relax by minimization of the Hellmann-Feynman force to a tolerance of less than 0.03 eV/Å. In the k-point sampling routine, a $2\times2\times2$ Monkhorst-Pack[31] mesh is used for supercell calculations. However, for the band structures calculations, the unit cell (consisting of two NH_3BH_3 molecules) was used with a much larger k-point sampling, i.e., a $15\times15\times15$ mesh. For the molecular calculations, periodic boundary conditions within a large supercell of $15\times15\times15$ Å was used in order to represent the isolated species. Bader analysis was performed on the molecular and solid AB system.[32] This analysis was performed using a grid-based algorithm.[33] In order to arrive at accurate Bader surfaces, the analysis is performed on the total charge density. The core charge which is associated with the PAW pseudopotentials are added to the self-consistently calculated valence charge. For a supercell, the defect formation energy is defined as[34]

$$\Delta H_f = E_{\text{tot}}(D^q) - E_{\text{tot}}(0) + \Sigma \Delta n_x \mu_x + qE_{\text{F}}, \tag{1}$$

where $E_{\text{tot}}(D^q)$ is the total energy of the cell with defect D in the charge state q. $E_{\text{tot}}(0)$ is the total energy of the cell without any defect and Δn_x is the number of atoms from species x being removed from a defect-free cell, to its respective reservoir with chemical potential μ_x, to form the defect cell. The chemical potential reflects the availability (or elemental partial pressure) of each element.

In order for equilibrium growth to occur, it is required that

$$\mu_{\text{AB}} = \mu_{\text{NH}_3} + \frac{1}{2}\mu_{\text{B}_2\text{H}_6}, \tag{2}$$

where μ_{AB}, μ_{NH_3}, and $\mu_{\text{B}_2\text{H}_6}$ are the chemical potentials of ammonia borane, the natural phase of NH_3 (ammonia), and the natural phase of BH_3 (diborane), respectively. Diborane is lower in energy than an isolated BH_3 and consists of two BH_3's bonded to each other by two bridging hydrogen.[35] The calculated energies per formula unit of AB, NH_3, and $\frac{1}{2}B_2H_6$ are −37.79, −19.60, and −17.06 eV (with respect to the neutral phase of each element), respectively. These calculated energies of the natural states of NH_3 and $\frac{1}{2}B_2H_6$ serve as upper bounds on their respective chemical potentials. The two limiting cases for this system are for growth under BH_3-rich conditions (NH_3 poor) and growth under NH_3-rich conditions. Under BH_3-rich conditions, $\frac{1}{2}\mu_{\text{B}_2\text{H}_6}=-17.06$ eV (maintaining BH_3's upper bound) which fixes μ_{NH_3} at −20.73 eV ($=\mu_{\text{AB}}-\frac{1}{2}\mu_{\text{B}_2\text{H}_6}$). Alternatively, under NH_3-rich conditions, $\mu_{\text{NH}_3}=-19.60$ eV (maintaining NH_3's upper bound) and $\frac{1}{2}\mu_{\text{B}_2\text{H}_6}$ falls to −18.19 eV ($=\mu_{\text{AB}}-\mu_{\text{NH}_3}$).

III. RESULTS AND DISCUSSION

A. Structural properties of ammonia borane

Ammonia borane has an orthorhombic crystal structure with two AB molecules per unit cell. The optimized supercell, containing 16 NH_3BH_3 molecules, has the following calculated lattice parameters: $a=5.29$, $b=4.89$, and $c=5.13$ Å. This is in good agreement with the values determined from neutron-diffraction experiments, 5.395, 4.887, and 4.986 Å.[36] The calculated sublimation energy of the molecular solid AB is 0.73 eV per formula unit. Since each H participates in two dihydrogen bonds, this gives an average bond strength of 0.12 eV. This is consistent with the previous DFT calculations of Morrison and Siddick, which determined a sublimation energy of 0.78 eV per formula unit,[19] but it falls short of the 0.94 eV, found from a combination of more sophisticated coupled cluster calculations and experiment.[22,23,37]

The molecules are held together by dihydrogen bonding. Bader charge analysis reveals that H, which are bonded to the N, carry a positive charge, while those bonded to the B carry a negative charge. For the molecule, these partial charges were found to be +0.62 e and −0.44 e for H_N and H_B, respectively. These partial charges were found to be quite consistent, the values of the bulk calculation differing from the molecule by less than 2%. These charge polarizations indicate that the basic bonding mechanism (dihydrogen bonding) of this material is represented in the DFT calculations. While every H in the system participates in the bonding, not all three H on NH_3 (nor on BH_3) are equivalent. Each NH_3 (and BH_3) has two equivalent H atoms and one inequivalent H atom. A top down view of a monolayer of bulk AB is shown in Fig. 1. In the figure, the dihydrogen bonds are explicitly shown and the equivalent and inequivalent H are labeled. There are three different bond lengths, $H_N^{(2)}\cdots H_B^{(1)}$, $H_N^{(1)}\cdots H_B^{(2)}$, and $H_N^{(2)}\cdots H_B^{(2)}$; which are found to be 1.89, 2.19, and 2.22 Å, respectively. The calculated bond lengths of the AB molecule and solid are summarized in Table I. As can be seen, the values calculated here are very consistent with previous DFT calculations,[18,19] and generally quite close to experiment with a largest error of approximately 6%. However, it should be noted that the DFT calcu-

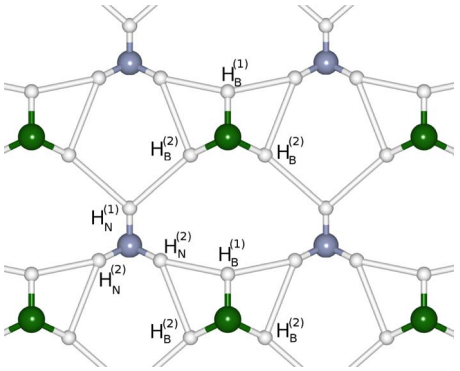

FIG. 1. (Color online) Top view of a monolayer of AB. A-B bonds (not shown) are approximately pointing into the page and dihydrogen bonds are explicitly shown. There are two equivalent H atoms (labeled $H_B^{(2)}$) and one inequivalent H atom (labeled $H_B^{(1)}$) for each BH_3 group. Similarly, there are two equivalent H atoms (labeled $H_N^{(2)}$) and one inequivalent H atom (labeled $H_N^{(1)}$) for each NH_3 group. Each H atom participates in two dihydrogen bonds.

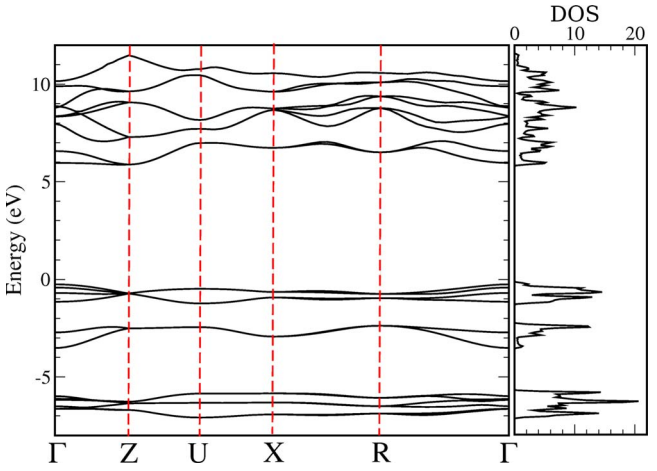

FIG. 2. (Color online) The left panel contains the calculated band structure of the ground state of ammonia borane (orthorhombic) using a two-molecule unit cell and a $15\times15\times15$ k-point sampling to obtain converged self-consistent charge density. The right panel is the complete electron density of states, in arbitrary units.

lations predict essentially unchanged B-H and N-H bond lengths in the solid state, failing to produce the observed B-H bond-length contraction.

Figure 2 shows the calculated electronic band structures (left panel) along with the density of states (right panel). The band structures indicate that solid AB has an indirect band gap [the conduction-band minimum (CBM) at Z and the valence-band maximum (VBM) at Γ] of 6.0 eV, which is larger than the calculated highest occupied molecular orbital (HOMO) to the lowest unoccupied molecular orbital (LUMO) gap of 5.0 eV. Although currently there is no experimental results on the band gap of solid AB, we can still put this material firmly in the realm of an insulator. This is because the band gaps obtained from similar calculations are always equal or smaller than the true gaps, due to the well-known DFT band-gap underestimation.

To gain basic understanding on the electronic structures, we compare the density of states (DOS) of AB to the calculated DOS of a NH_3BH_3 molecule (Fig. 3). For NH_3BH_3 molecule, the DOS simply show discrete molecular energy levels. In addition, we also plot the decomposed partial density of states (PDOS) to identify the characteristic of each energy level. From the PDOS of NH_3BH_3 molecule (Fig. 4), the lowest energy state at −17.2 eV (with respect to the HOMO level) is composed of N s and H_N s states. Therefore, the state is clearly an N-H bonding state. The next state at −7.1 eV is doubly degenerate and composed of N p and H_N s states, which means it is another N-H bonding state. These three states [−17.2 eV(1x) and −7.1 eV(2x)] are the bonding states between three H_N s and N sp^3. The next state at −6.1 eV, composed of N p and B s, is the N-B bond with a small mixture of H_B. At −2.1 eV, there is a state composed of N p and B sp with a small mixture of H_B. This state is another N-B bond. The highest occupied state (HOMO) is doubly degenerate and composed of B p and three H_B.

As the molecules interact with each other in the molecular solid NH_3BH_3, the DOS is broadened (Fig. 3). Note that the energy in Fig. 3 is referenced to the valence-band maximum of NH_3BH_3 solid. We can see that the characters of the low-

TABLE I. Comparison of the calculated bond lengths (in Å) of molecular and bulk phase AB with similar DFT calculations and experiment.

	Bulk			Molecule	
Bond	This work	Calc.[a,b]	Exp.[c]	This work	Exp.[d]
B-N	1.59	1.59[a] 1.58[b]	1.58	1.65	1.65
$B\text{-}H^{(1,2)}$	1.22,1.23	1.22[a]	1.15,1.18	1.22	1.21
$N\text{-}H^{(1,2)}$	1.03,1.03	1.03[a]	1.07,0.96	1.02	1.01
$H_N^{(2)}\cdots H_B^{(1)}$	1.89	1.91[b]	2.02		
$H_N^{(1)}\cdots H_B^{(2)}$	2.19	2.20[a] 2.17[b]	2.21		
$H_N^{(2)}\cdots H_B^{(2)}$	2.22	2.27[b]	2.23		

[a]Miranda and Ceder (Ref. 18).
[b]Morrison and Siddick (Ref. 19).
[c]Neutron diffraction study of Klooster *et al.* (Ref. 36).
[d]Microwave spectra of the gas phase of Thorne *et al.* (Ref. 38).

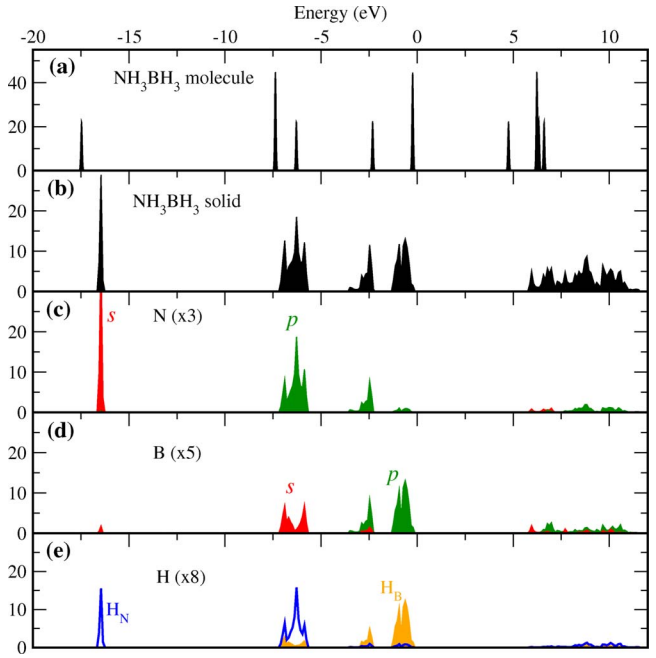

FIG. 3. (Color online) Electron density of states (DOS), in arbitrary units, of (a) NH_3BH_3 molecule and (b) molecular solid NH_3BH_3. (b)–(d) Site decomposed DOS. For each atom center, the local partial DOS in a sphere radius R (N:R=0.74 Å, B:R =0.91 Å, H:R=0.37 Å) is calculated. The partial DOS plots are scaled up by a factor given in the parentheses for clarity.

est energy state is still the same as that of NH_3BH_3 molecule, i.e., a localized bonding state composed of N s and H_N s states, with the exception that the DOS of the solid is slightly broader. At higher energy, the molecular states interact with each other due to the formation of dihydrogen bonds between H_N and H_B and the band dispersion. As can be seen from Fig. 2, the band dispersion is of the order of 2 eV. As a results, any molecular levels that are close together in energy

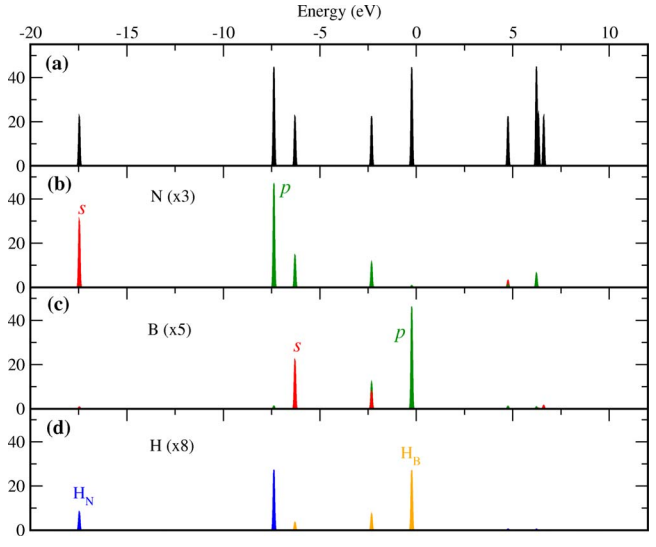

FIG. 4. (Color online) (a) Electron density of states (DOS), in arbitrary units, of NH_3BH_3 molecule. The energy is referenced to the HOMO level. (b)–(d) Site decomposed DOS.

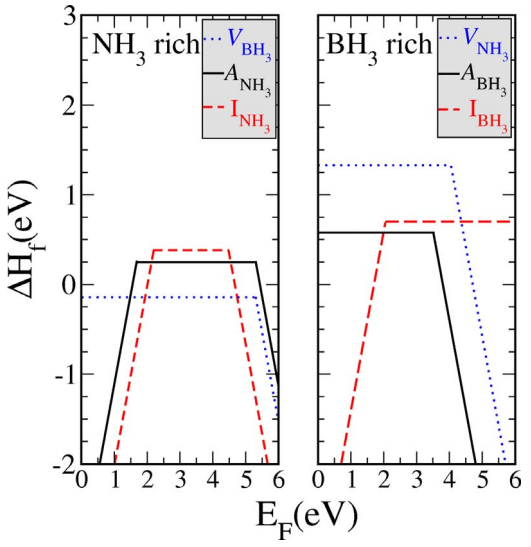

FIG. 5. (Color online) The calculated formation energies of native defects in ammonia borane. The left panel is under NH_3-rich conditions and the right panel is under BH_3-rich conditions. The Fermi energy is referenced from the VBM, and the plots range over the calculated band gap.

are merged. For instance, the molecular bonding states between N-p and H_N are no longer isolated but are merged with the higher state (N-p and B-s hybridization with a small mixture of H_B for the molecular case). The higher states that are more distinctive in energy are not merged but are significantly broadened. It is interesting to note that the valence-band and conduction band are both quite flat (especially between Γ to Z direction). This is because the interactions between the molecular units are much weaker than that of the traditional solids, leading to a relatively small energy dispersion of the band structures.

B. Formation energies and charge states of native defects

The formation energies of various defects were calculated as a function of Fermi energy. Figure 5 shows the main results for the ammonia and borane related defects for the different growth conditions. Their formation energies are shown in Table II. Here, we present the results of two extreme conditions: NH_3-rich (BH_3-poor) and BH_3-rich (NH_3-poor). The actual equilibrium growth conditions have to occur between these two extreme cases. It can be seen that none of the defects in positive charge (defects with a positive slope in Fig. 5) cross with any of the defects in negative charge (negative slope). This means there will not be significant concentration of charged defects for an undoped sample as this would not allow for charge conservation.

The formation energies of several neutral native defects in AB were found to be surprisingly low at appropriate growth conditions. The NH_3-rich growth conditions (Fig. 5, left panel) provide the best opportunity for some native defects, which effectively increase the NH_3 stoichiometry, to form. $V^0_{BH_3}$, $A^0_{NH_3}$, and $I^0_{NH_3}$ all have formation energies of less than 0.4 eV which are very low. The negative formation energy of $V^0_{BH_3}$ (of −0.14 eV) indicates that the system reduces energy

TABLE II. Calculated formation energies of ammonia and borane related defects. The first column is the name of the defect. The next six columns are the calculated formation energies for the various charge states [(−2), (0), and (+2)] for E_F=0 (relative to the VBM). Although (+1) and (−1) charge states were calculated, they were not found to be stable for any of these defects. The last two columns are the Fermi energies at which the stable charge state changes from (+2) to (0) and then from (0) to (−2).

	ΔH_f (eV)						ϵ	
	NH_3 rich			BH_3 rich				
Defect	−2	0	+2	−2	0	+2	(+2/0)	(0/−2)
A_{BH_3}	10.24	2.84	1.09	7.97	0.57	−1.17	0.88	3.70
I_{BH_3}	14.08	1.84	−2.65	12.94	0.71	−3.78	2.25	
V_{BH_3}	10.84	−0.14	−0.52	11.97	0.99	0.61	0.19	5.49
A_{NH_3}	11.23	0.25	−3.48	13.50	2.52	−1.21	1.87	5.49
I_{NH_3}	9.71	0.38	−4.39	10.84	1.52	−3.26	2.39	4.66
V_{NH_3}	10.92	2.46	2.65	9.79	1.32	1.53		4.24

by forming $V^0_{BH_3}$, rendering AB unstable under NH_3-rich growth conditions. To avoid forming AB crystal full of V_{BH_3} defects, μ_{NH_3} has to be reduced at least to the point where the energy of $V^0_{BH_3}$ turns zero. This means, strictly speaking, the extreme μ_{NH_3} has to be redefined to −19.74 (= −19.60−0.14) eV and the formation energies of $V^0_{BH_3}$, $A^0_{NH_3}$, and $I^0_{NH_3}$ would increase by 0.14, 0.28, and 0.14 eV, respectively. Since the differences are quite small, we choose to present our numerical results under extreme NH_3-rich growth conditions for simplicity. If needed, the formation energies of defects under other conditions (different chemical potentials), including the case discussed above, can be recalculated using Eq. (1).

The BH_3-rich growth conditions (Fig. 5, right panel) provide the best opportunity for some native defects, which effectively increase the BH_3 stoichiometry, to form. The three defects with the lowest formation energy are $A^0_{BH_3}$, $I^0_{BH_3}$, and $V^0_{BH_3}$ with formation energies of 0.57, 0.71, and 0.99 eV, respectively. The formation energies are slightly higher than $V^0_{BH_3}$, $A^0_{NH_3}$, and $I^0_{NH_3}$ under NH_3-rich growth conditions (even after the redefined extreme μ_{NH_3}). Nevertheless, the formation energies of these defects are still quite low, especially when comparing with the neutral defects in traditional wide-gap materials. The structure of each of these defects as well as a discussion of the chemistry in the different charge states will be provided in the next section.

C. Structure and stability of native defects

1. Ammonia antisite (A_{NH_3})

A_{NH_3} refers to the defect where a BH_3 group is replaced with NH_3. The relaxed structure of the neutral defect is shown in Fig. 6(f). The enlarged version is also shown in Fig. 7 (middle), for direct comparison of the structure in other charge states. For the neutral charge state, the two NH_3 are essentially just separated into two ammonia molecules; each of which have a localized lone pair on the N atom. The two NH_3 do not directly bond, but instead orient themselves such that their lobes point directly away from each other. This defect is further stabilized by the orientation of each NH_3 with respect to the neighboring atoms. The lone pair of antisite NH_3 is pointed midway between two positively

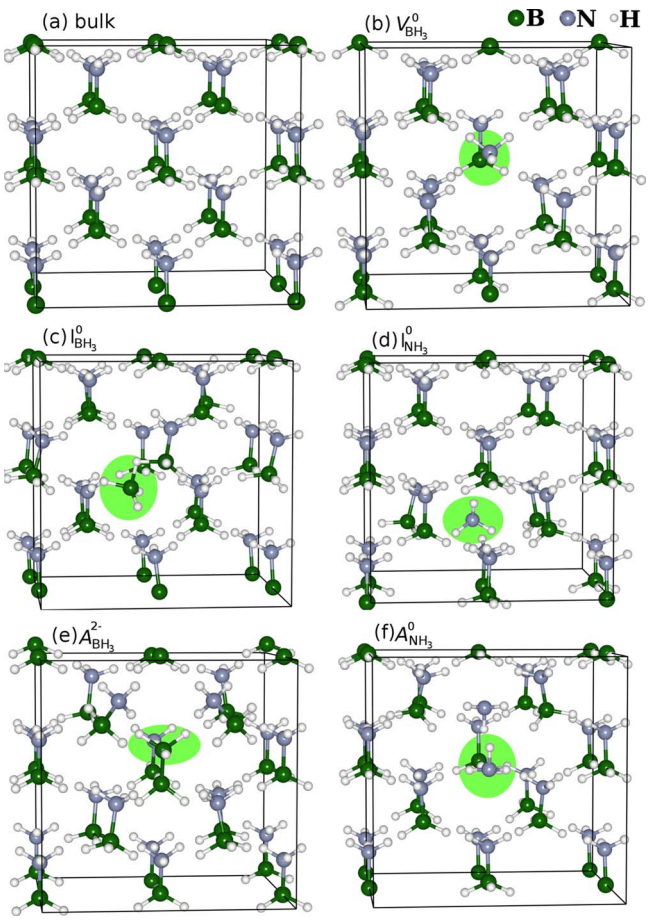

FIG. 6. (Color online) (a) Atomic structure of bulk ammonia borane and (b)–(f) defects. The dark (green) atoms are B, the gray atoms (blue) are N, and the small white atoms are H. In the case of each defect, the location of the defect has been highlighted in gray (green).

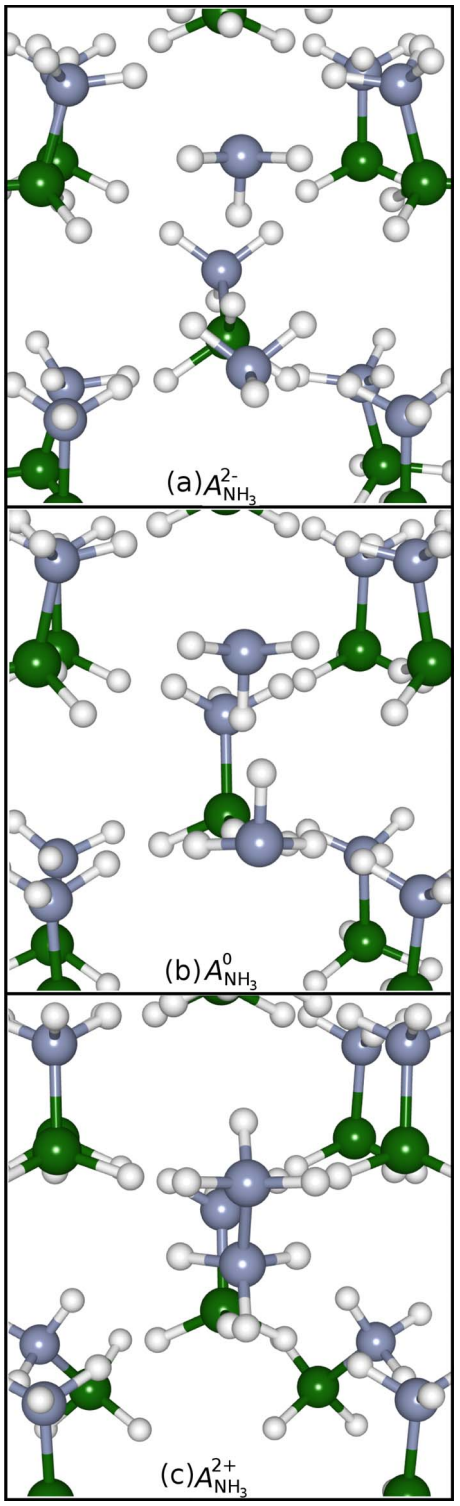

FIG. 7. (Color online) Lowest energy structure of the different charge states of the A_{NH_3} defect; $A^{2-}_{NH_3}$ (a), $A^{0}_{NH_3}$ (b), and $A^{2+}_{NH_3}$ (c). Direct N-N bonding is only possible when the NH_3 lone pairs have been depleted, i.e., in the (+2) charge state.

charged adjacent H which are bound to N (H_N), yielding a N..H distance of 2.23 Å. This is only slightly shorter than the 2.30 Å hydrogen bond length of the isolated NH_3 dimer, as determined from highly accurate CCSD(T) calculations.[39] Additionally, the other associated NH_3, which is at the correct lattice position, reorients to increase the number of dihydrogen bonds; one of its H is located midway between 3 H_B (each 2.25 Å away); and the other two each point toward two H_B about 2.30 Å away.

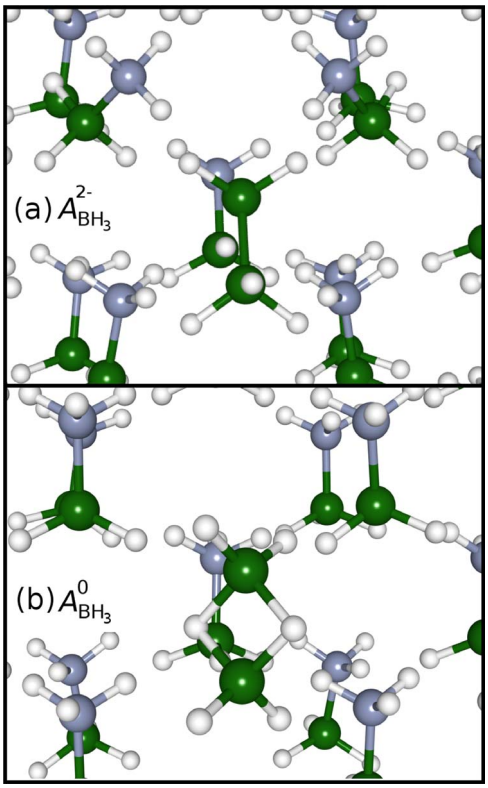

FIG. 8. (Color online) Lowest energy structure of the stable charge states of the A_{BH_3} defect; $A^{2-}_{BH_3}$ (a), and $A^{0}_{BH_3}$ (b). The top figure is a zoom-in version of Fig. 6(e) and is included for a direct comparison with the neutral charge state (b). In the neutral charge state, B_2H_6 forms the familiar diborane structure, where two BH_2's are connected by two bridging hydrogen atoms. In the (−2) charge state (a), the lowest energy structure was found to have direct B-B bonding. The antisite BH_3 causes the two nearby NH_3BH_3 molecules to rotate more than 45°, so that the H from the nearby NH_3 groups can bind to the antisite BH_3.

On the other hand, in the (+2) charge state (Fig. 7, bottom), each of these lobes are half empty, allowing for the formation of a direct N-N bond. The N-N bond length is slightly smaller (1.44 Å) than the B-N bond length (1.59 Å). The geometry of $(N_2H_6)^{2+}$ is similar to that of an ethane (C_2H_6) molecule. All six N-H bonds are almost equal (in the range of 1.05–1.07 Å) and the dihedral angles are in the range of 55–62°. Furthermore, The $(N_2H_6)^{2+}$ rotates such that all of the H point toward H on B.

The charge stability of this defect is shown in Fig. 5 (left). This defect is likely to form under NH_3-rich conditions, the neutral defect having a formation energy of only 0.25 eV (this increases to 2.5 eV under BH_3-rich conditions).

2. *Borane antisite* (A_{BH_3})

The relaxed structures of A_{BH_3} in the (−2) and the neutral charge state are shown in Fig. 8 (top) and (bottom), respec-

tively. Because the defect increases the number of BH_3 molecules in the material, the defect is much more likely to form under BH_3-rich (ΔH_f=0.57 eV) conditions than NH_3-rich (ΔH_f=2.84 eV) conditions.

In the neutral charge state, B_2H_6 forms the familiar diborane structure, where two BH_3 molecules are connected by two bridging hydrogen atoms. These are the three-center two-electron bonds which are ubiquitous in boron chemistry.[40,41] This structure is quite stable (isolated diborane is in fact the reference energy structure of BH_3 for the formation energy calculations) and is the most easily formed neutral defect under BH_3-rich conditions, having a formation energy of only 0.57 eV.

On the other hand, the structure of the defect in (−2) charge state is different from the neutral one. For the (−2) charge state, the antisite B binds directly to another B, which sits at the lattice site, forming BH_3BH_3. The geometry of $(BH_3BH_3)^{2-}$ is similar to that of an ethane molecule with the exception that all of the bonds are longer. All six B-H bonds are almost equal (1.24–1.25 Å) and the dihedral angles are all within the range of 58–62°. Although the B atom stays almost perfectly substitutional for N, there are substantial relaxations of the neighboring atoms. This is due to the fact that the H atoms on the antisite BH_3 carry a partial negative charge instead of the partial positive charge that would exist if they were part of a NH_3 group. So the antisite BH_3 repel the two nearby BH_3 and attract the H of the nearby NH_3 groups. This results in a clear rotation (more than 45°) of the adjacent BH_3NH_3 molecules [Fig. 8(a)]. In this case, the excess electrons seem to be concentrated on the antisite H, strengthening the dihydrogen bonding. The smallest $A_{BH_3}\cdots NH_3$ dihydrogen bond length is 1.55 Å, which is much smaller than that of bulk AB (1.97 Å).

3. Ammonia vacancy (V_{NH_3})

The NH_3 vacancy is the defect which remains when an NH_3 is removed from one the NH_3BH_3 molecules in solid AB. This is equivalent to a BH_3 sitting in a (AB) molecular vacancy. The neutral charge state of this defect has rather high formation energy, ranging from 1.3 to 2.4 eV in BH_3-rich to BH_3-poor conditions, making it unlikely to form in any substantial quantity. In the neutral charge state, the remaining BH_3 in the molecular vacancy exists as it would in vacuum, i.e., as borane with a trigonal planar shape [Fig. 9, (bottom)]. Isolated BH_3 is electron deficient, therefore one should not expect that its H atoms should possess the partial negative charge as they do in NH_3BH_3. Indeed, while one of the H atoms on borane might participate in dihydrogen bonding (though it could be accidental), with a H-H distance of 2.06 Å from two nearby H_N atoms. The other two are about 2.6 Å away from nearby H_N even though this distance can easily be reduced. In order for the NH_3 vacancy to exist in quantity, the Fermi energy would have to exceed 4.2 eV (above the VBM). This is where the (−2) charge state becomes stable.

In the (−2) charge state, BH_3 is no longer electron deficient and takes on a trigonal pyramidal structure (Fig. 9, top). The charge separation is regained, and its H once again posses a partial negative charge. The B stays nearly on site, and

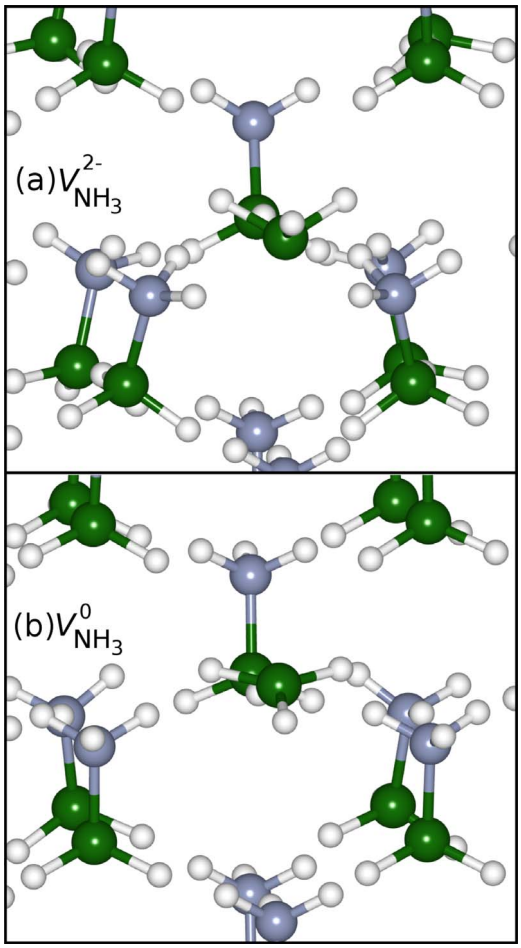

FIG. 9. (Color online) The lowest energy configuration of the two charge states of V_{NH_3}; $V_{NH_3}^{2-}$ (a) and $V_{NH_3}^{0}$ (b). For $V_{NH_3}^{0}$, the BH_3 in the molecular vacancy exists as it would in vacuum, as borane, which is trigonal planar. For $V_{NH_3}^{2-}$, the isolated BH_3 regains a trigonal pyramidal structure.

the H orient themselves to maximize the number of dihydrogen bonds. Two of the H atoms form two dihydrogen bonds with lengths of 1.95 and 2.19 Å and the third H forms three dihydrogen bonds; two with length of 1.98 Å and one with length of 1.92 Å.

4. Borane vacancy (V_{BH_3})

The BH_3 vacancy has the lowest formation energy among the neutral native defects investigated here. It is primarily a neutral defect, the calculation shows that it becomes (−2) charge state only for Fermi energies near the CBM (5.49 eV above the VBM). $V_{BH_3}^{0}$ has a formation energy of 1.00 eV (under BH_3-rich conditions) and −0.14 eV (under NH_3-rich conditions). This calculated negative formation energy of the neutral defect implies that AB is unstable under certain growth conditions, namely, under NH_3-rich conditions.

The relaxed structure of $V_{BH_3}^{0}$ is shown in Fig. 10 (bottom). The remaining NH_3 in the molecular vacancy exists as ammonia with the lone pair populated and trigonal pyramidal structure. The NH_3 shifts to the center of the molecular vacancy and reorients in order to minimize energy. Instead of

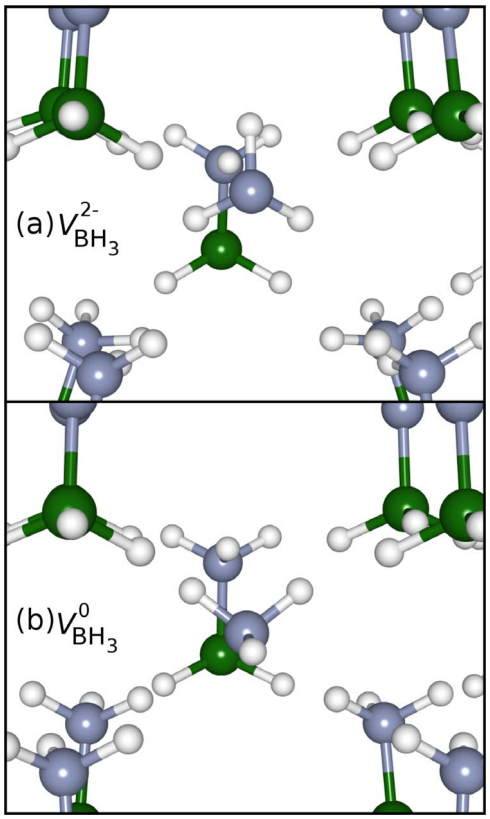

FIG. 10. (Color online) The lowest energy configuration of the two charge states of V_{BH_3}; $V_{BH_3}^{2-}$ (a) and $V_{BH_3}^{0}$ (b). For $V_{BH_3}^{0}$, the NH_3 in the molecular vacancy exists as ammonia the lone pair populated and trigonal pyramidal structure.

maximizing the number of dihydrogen bonds, the NH_3 orients so that its lone pair is located midway between the H of two nearby NH_3 groups, which would have bonded to the missing BH_3. This is essentially hydrogen bonding with the N-H distance of 2.28 Å, nearly identical to that of the NH_3 dimer. While this hydrogen bonding occurs at the expense of one of the H forming any dihydrogen bonds, the other two H do still each form two dihydrogen bonds with bond lengths of 2.07 and 2.31 Å.

The chemistry involved in the (−2) charge state is much less apparent. The N stays near the proper lattice site, but does not participate in dihydrogen bonding, see Fig. 10 (top). Instead, it orients itself so that none of its H are near any of the H on B (the closest distance being over 2.9 Å away). Furthermore, the lone pair which participated in hydrogen bonding in the neutral case is nowhere near a N bonded H, almost 3.5 Å away.

5. Ammonia interstitial (I_{NH_3})

Interstitial NH_3 can form fairly easily under NH_3-rich conditions with a formation energy for the neutral charge state of only 0.38 eV (1.52 eV under BH_3-rich conditions). The relaxed structure of this defect is shown in Fig. 11 (top). Although NH_3 does not covalently bond to any atoms in the lattice, its orientation substantially lowers the energy. Much like NH_3 in the molecular vacancy, the highly electronega-

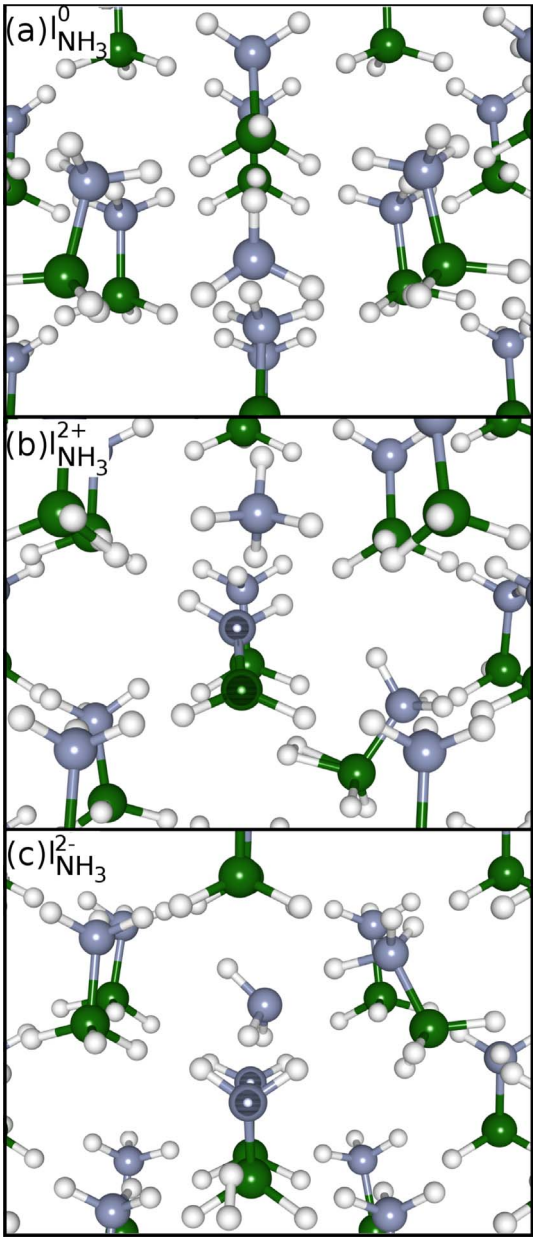

FIG. 11. (Color online) I_{NH_3} in the (0) (a), (+2) (b), and (−2) (bottom) charge states. The atoms (either B or N) which are darkened in the center have lost a H due to the presence of the defect. In the (+2) and (−2) charge states, the relaxed structure involves considerable rearrangement of the host lattice. In the (+2) charge state, two H come of an adjacent BH_3NH_3. One of these H bond directly to I_{NH_3}, while the other bonds to a nearby H (from BH_3), forming NH_3BH_4. In the (−2) charge state, a H comes off two separate N and forms interstitial H_2. This energy cost is partially offset by the formation of two strong hydrogen bonds with I_{NH_3}.

tive N carries a partial negative charge and forms a hydrogen bond with a H (from a nearby NH_3), albeit a stronger one with a shorter bond length of 1.89 Å. Additionally, the three positively charged H participate in dihydrogen bonding with H (from adjacent BH_3 groups). Two of the H form only single dihydrogen bonds, though they are stronger than those found elsewhere in the lattice, having relatively short bond lengths of 1.68 and 1.75 Å. The third H forms three weaker

dihydrogen bonds with the bond lengths of 2.04, 2.20, and 2.11 Å.

The (+2) and (−2) charge states yielded unexpected results. In both of these charge states, I_{NH_3} was found to be highly reactive with the lattice. For the (−2) charge state, the initial structure relaxed to the configuration shown in Fig. 11 (bottom) in which two H atoms vacate different N and form interstitial H_2. Although this structure seems strange since two covalent bonds (N-H) are broken and only one (H-H) is reformed, it is relatively low in energy. In addition to the formation of a covalent H-H bond, the structure is further stabilized by the formation of two hydrogen bonds (1.54 and 1.81 Å in length). It should be noted that these bond lengths are substantially shorter than would be expected for a NH_3..NH_3 hydrogen bond.[39,42] $I^{2-}_{NH_3}$ is the most stable negatively charged defect under NH_3-rich growth conditions, becoming stable for $E_F > 4.66$ eV.

For the (+2) charge state, once again two covalent bonds are broken. However, in this case they are both reformed. A nearby NH_3BH_3 molecule donates two of its H (one from B and one from N), leaving a planar NH_2BH_2. The removal of an electron from the lone pair of I_{NH_3} allows for the bonding of an additional H, forming NH_4^+. The other goes to the B of a nearby NH_3BH_3. While there are four H in the vicinity of this nearby B, they do not all directly bind. Instead it seems as if only two are directly bound, having a bond length of 1.2 Å. The other two H atoms exist as H_2 (H-H bond distance of 0.85 Å) and an elongated bond length with respect to the B (1.35 and 1.4 Å).

6. *Borane interstitial* (I_{BH_3})

In the neutral charge state, interstitial BH_3 is similar to a bond centered defect, where the interstitial BH_3 group bridges an existing dihydrogen bond. While it breaks the dihydrogen bond, the structure is stabilized in two ways. First, I_{BH_3} forms a hydrogen bridged bond with the BH_3 side of a NH_3BH_3 molecule, see Fig. 12 (top). This is a three-center two-electron bond, which is very common in B chemistry.[40,41] The B reference structure, diborane, contains two such bridging hydrogen. Second, the dihydrogen bonds are reconstructed by I_{BH_3}. For E_F of less than 2.25 eV above the VBM, the (+2) charge state is more stable. In the (+2) charge state, I_{BH_3} donates a H atom to the host lattice in order to form two hydrogen bridged bonds with a BH_3, see Fig. 12 (bottom). The resulting structure is very similar to diborane, having two bridging hydrogen, but with one of the H substituted with NH_3.

IV. CONCLUSIONS

Using first-principles methods, we have calculated the atomic structures and formation energies for a number of native defects in ammonia-borane including $V_{BH_3}(V_{NH_3})$, $A_{BH_3}(A_{NH_3})$, and $I_{BH_3}(I_{NH_3})$. We found that the formation energies for the charge-neutral defects, depending on the growth conditions, can be surprisingly low. For example, at the NH_3-rich growth conditions, the formation energies for $V^0_{BH_3}$, $A^0_{NH_3}$, and $I^0_{NH_3}$ are −0.14, 0.25, and 0.38 eV, respectively. A slightly negative formation energy for $V^0_{BH_3}$ indicates that even the range of the chemical potential for equilibrium growth of the AB can be modified by the defect formation. At the BH_3-rich growth conditions, although neutral defects in general have higher formation energies, several of them can still maintain relatively low energies, 0.57, 0.71, and 0.99 eV, respectively, for $A^0_{BH_3}$, $I^0_{BH_3}$, and $V^0_{BH_3}$.

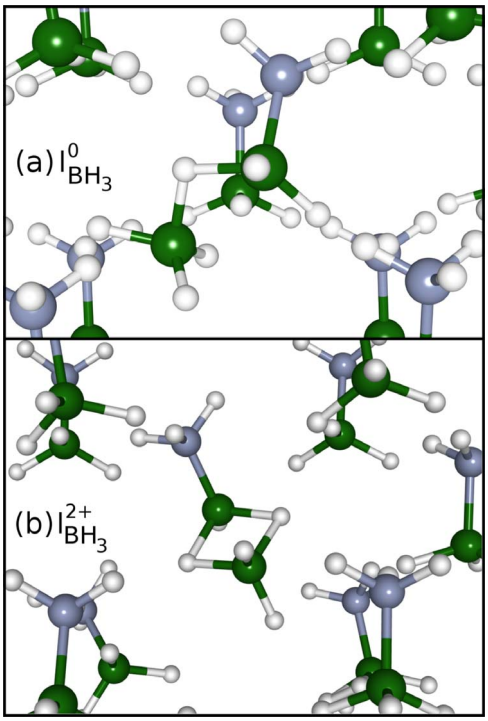

FIG. 12. (Color online) $I^0_{BH_3}$ (a) and $I^{2+}_{BH_3}$ (b). In the neutral charge state, the interstitial BH_3 forms a bond centered type configuration. While it breaks a dihydrogen bond, it reconstructs it on both sides. On one side, I_{BH_3} forms a H bridged bond with a BH_3 group from a BH_3NH_3. While on the other side, one of its H's participate in two dihydrogen bonds. In the (+2) charge state, I_{BH_3} donates a H to the host lattice in order to form two hydrogen bridged bonds with a BH_3. The resulting structure is very similar to diborane, but with one of the H substituted with NH_3.

The relative ease of neutral defect formation here can be understood in terms of the molecular nature of the AB solid, which is made of the NH_3 and BH_3 molecular building blocks. In addition, the ease of the defect formation can be traced back to a rich variety of bonding types in this system. The defect-free AB solid can be described by a mixture of dative N-B bonds for intramolecular bonding and much weaker dihydrogen bonds responsible for intermolecular bonding. While the presence of a native defect breaks the strong N-B bond, it also allows for the formation of intermediate strength hydrogen bonds (stronger than the dihydrogen bonds) to make up for the energy increase and hence lowers the overall system energy. The lone pair on the NH_3 makes it particularly prone to the formation of hydrogen bonds, explaining why the NH_3-related defects are so low in energy.

While the AB molecular solid model is successful in explaining most of the native defects that we have studied (in which the NH_3 and BH_3 units maintain their initial molecular

forms), this view breaks down for a number of charged interstitials. For example, the introduction of $I^{2+}_{NH_3}$, $I^{2-}_{NH_3}$, and $I^{2+}_{BH_3}$ results in complicated structures involving the release of H. In particular, $I^{2+}_{NH_3}$ and $I^{2+}_{BH_3}$ form complexes with the release of interstitial atomic H, whereas $I^{2-}_{NH_3}$ forms a complex with the release of interstitial H_2. Understanding the mechanisms behind these defect formations may be of particular interest in the context of hydrogen storage. Given that $I^{2+}_{NH_3}$ and $I^{2+}_{BH_3}$ have low formation energies for Fermi level near the VBM but $I^{2-}_{NH_3}$ have low energy for Fermi level near the CBM, these findings open up the possibility of changing hydrogen desorption energetics by shifting the system Fermi energy via extrinsic doping, carrier injection, or photoexcitation.

ACKNOWLEDGMENTS

We thank Ping Chen (National University of Singapore) for much useful discussion. We also gratefully acknowledge the generous amount of computer time provided by Rensselaer Polytechnic Institute's Computational Center for Nanotechnology Innovations. S.L. acknowledges support from NANOTEC (Grant No. NN-B-22-DI2-20-51-09) and the Commission on Higher Education, Thailand (CHE-RES-RG Theoretical Physics).

*westd2@rpi.edu

[1] Frances H. Stephens, Vincent Pons, and R. Tom Baker, Dalton Trans. **2007**, 2613.
[2] E. Mayer, Inorg. Chem. **11**, 866 (1972).
[3] M. G. Hu, J. M. Van Paasschen, and R. A. Geanangel, J. Inorg. Nucl. Chem. **39**, 2147 (1977).
[4] G. Wolf, J. C. van Miltenburg, and U. Wolf, Thermochim. Acta **317**, 111 (1998).
[5] N. Hess, M. Bowden, V. Parvanov, C. Mundy, S. Kathmann, G. Schenter, and T. Autrey, J. Chem. Phys. **128**, 034508 (2008).
[6] G. Wolf, J. Baumann, F. Baitalow, and F. P. Hoffmann, Thermochim. Acta **343**, 19 (2000).
[7] F. Baitalow, J. Baumann, G. Wolf, K. Jaenicke-Rler, and G. Leitner, Thermochim. Acta **391**, 159 (2002).
[8] J. Baumann, F. Baitalow, and G. Wolf, Thermochim. Acta **430**, 9 (2005).
[9] A. Gutowska, L. Li, Y. Shin, C. M. Wang, X. S. Li, J. C. Linehan, R. S. Smith, B. D. Kay, B. Schmid, W. Shaw, M. Gutowski, and T. Autrey, Angew. Chem. Int. Ed. **44**, 3578 (2005).
[10] U. S. Dept. of Energy, EERE (http://www.eere.energy.gov/hydrogenandfuelcells/mypp/pdfs/storage.pdf).
[11] S. De Benedetto, M. Carewska, C. Cento, P. Gislon, M. Pasquali, S. Scaccia, and P. P. Prosis, Thermochim. Acta **441**, 184 (2006).
[12] F. Stephens, R. Baker, M. Matus, D. Grant, and D. Dixon, Angew. Chem. Int. Ed. **46**, 746 (2007).
[13] R. Keaton, J. Blacquiere, and R. Baker, J. Am. Chem. Soc. **129**, 1844 (2007).
[14] M. Bluhm, M. Bradley, R. Butterick, U. Kusari, and L. Sneddon, J. Am. Chem. Soc. **128**, 7748 (2006).
[15] A. Feaver, S. Sepehri, P. Shamberger, A. Stowe, T. Autrey, and G. Cao, J. Phys. Chem. B **111**, 7469 (2007).
[16] S. Sepehri, B. B. Garcia, Q. Zhang, and G. Cao, in *Materials and Technology for Hydrogen Storage*, edited by G-A. Nazri, C. Ping, A. Rougier, and A. Hosseinmardi MRS Symposia Proceedings No. 1042E (Materials Research Society, Warrendale, 2008), p. 1042-S07-01.
[17] Z. Xiong, C. Yong, G. Wu, P. Chen, W. Shaw, A. Karkamkar, T. Autrey, M. Jones, S. Johnson, P. Edwards, and W. David, Nature Mater. **7**, 138 (2008).
[18] C. Miranda and G. Ceder, J. Chem. Phys. **126**, 184703 (2007).
[19] C. A. Morrison and M. M. Siddick, Angew. Chem. Int. Ed. **43**, 4780 (2004).
[20] V. Nguyen, M. Matus, D. Grant, M. Nguyen, and D. Dixon, J. Phys. Chem. A **111**, 8844 (2007).
[21] M. Nguyen, V. Nguyen, M. Matus, G. Gopakuman, and D. Dixon, J. Phys. Chem. A **111**, 679 (2007).
[22] Myrna H. Matus, Kevin D. Anderson, Donald M. Camaioni, S. Thomas Autrey, and David A. Dixon, J. Phys. Chem. A **111**, 4411 (2007).
[23] D. A. Dixon and M. Gutowski, J. Phys. Chem. A **109**, 5129 (2005).
[24] Y. Wang and J. P. Perdew, Phys. Rev. B **44**, 13298 (1991); J. P. Perdew, in *Electronic Structure of Solids '91*, edited by P. Ziesche and H. Eschring (Akademie Verlag, Berlin, 1991), p. 11.
[25] P. E. Blochl, Phys. Rev. B **50**, 17953 (1994).
[26] G. Kresse and D. Joubert, Phys. Rev. B **59**, 1758 (1999).
[27] VASP, 2003 at http://cms.mpi.univie.ac.at/vasp.
[28] G. Kresse and J. Hafner, Phys. Rev. B **47**, 558 (1993).
[29] G. Kresse and J. Furthmüller, Phys. Rev. B **54**, 11169 (1996).
[30] G. Kresse and J. Furthmüller, Comput. Mater. Sci. **6**, 15 (1996).
[31] H. J. Monkhorst and J. D. Pack, Phys. Rev. B **13**, 5188 (1976).
[32] R. F. W. Bader, *Atoms in Molecules: A Quantum Theory* (Oxford University Press, New York, 1990).
[33] http://theory.cm.utexas.edu/vtsttools/bader/; G. Henkelman, A. Arnaldsson, and H. Jnsson, Comput. Mater. Sci. **36**, 354 (2006); E. Sanville, S. D. Kenny, R. Smith, and G. Henkelman, J. Comput. Chem. **28**, 899 (2007).
[34] S. B. Zhang and J. E. Northrup, Phys. Rev. Lett. **67**, 2339 (1991).
[35] D. Feller, D. A. Dixon, and K. A. Peterson, J. Phys. Chem. A **102**, 7053 (1998).
[36] W. T. Klooster, T. F. Koetzle, P. E. M. Siegbahn, T. B. Richardson, and R. H. Crabtree, J. Am. Chem. Soc. **121**, 6337 (1999).
[37] J. Baumann, Ph.D. thesis, TU Bergakademi Freiberg, Germany, 2003; G. Wolf, in *W. E. Heraeus Seminar on Hydrogen Storage with Novel Nanomaterials* (Bad Honnef, Germany, 2005), http://www.h-workshop.uni-konstanz.de/pdf/Wolf_Gert.pdf
[38] L. R. Thorne, R. D. Suenram, and F. J. Lovas, J. Chem. Phys. **78**, 167 (1983).
[39] A. Daniel Boese, Amalendu Chandra, Jan M. L. Martin, and Dominik Marx, J. Chem. Phys. **119**, 5965 (2003).
[40] W. N. Lipscomb, Science **196**, 1047 (1977).
[41] W. N. Lipscomb, *Boron Hydrides* (Benjamin, New York, 1963).
[42] D. D. Nelson, Jr., G. T. Fraser, and W. Klemperer, J. Chem. Phys. **83**, 6201 (1985).